CHAPTER

6

A breast tissue characterization framework using PCA and weighted score fusion of neural network classifiers

* † ‡ §

*Department of Computer Science and Engineering, Galgotia Educational Institutions, Greater Noida, India †CSIR-CSIO, Chandigarh, India ‡Department of Computer Science and Engineering, GB Pant Institute of Engineering and Technology, Pauri, Garhwal, India §Department of Radi-

6.1 Introduction

Basically, the breast tissue density, i.e., breast tissue pattern is defined as the amounts of fatty and fibro glandular tissues present in the breast and considered as a major risk [1–17]. A dense breast has less percentage of fatty tissue and more in the case of fibrous tissue. The 4-class breast density clas- [12,18–22] Table 6.1. [23–28] is the most frequently used method for screening of breast abnormalities. Due to high specificity and sensitivity of mammography, the detection of small tumors and micro calcifications becomes easy. The breast tissue pattern characterization is clinically significant for atypical cases due to some superimposition of important visual information between images that belong to different breast tissue patterns (especially in the case of B2 and B3), so the characterizations between different breast tissue patterns can be considered as a difficult task.

The sample images belonging to B1, B2, B3, and B4 classes are obtained from the Fig. 6.1.

After an extensive review of the past studies, it has been found that development of computerized framework for breast density characterization using digital image processing methodology is significant due to (a) the variations in tissue pattern reflects variations in texture properties; hence, the classification of breast tissue pattern can be considered as the matter of textural description, and (b) it is clinically significant as most of the time lesions that are present behind the dense tissue fail

https://doi.org/10.1016/B978-0-12-818004-4.00006-6

Table 6.1 Breast density classification according to BIRADS classification

BIRADS class	Density (%)	Breast density
B1	00–25	Entirely fatty breast tissue
B2	26–50	Some fibroglandular breast tissue
B3	51–75	Heterogeneously dense breast tissue
B4	76–100	Extremely dense breast tissue

B1, *BIRADS-I;* B2, *BIRADS-II;* B3, *BIRADS-III;* B4, *BIRADS-IV.*

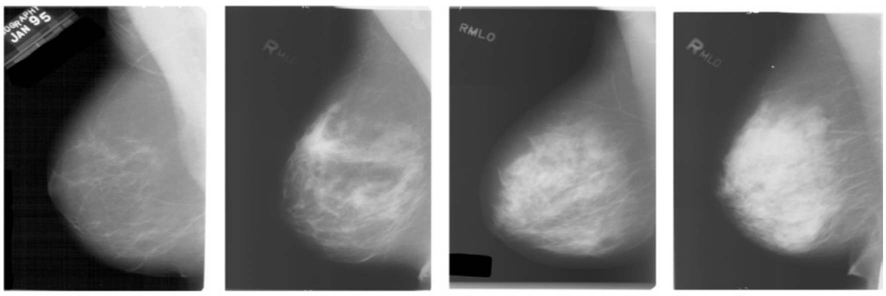

FIG. 6.1

Sample images of each class.

to get noticed during the screening process. The development of breast tissue char-
Fig. 6.2.
Fig. 6.2, it has been observed that the breast tissue characterization problem can be processed in three different ways. In this study, 4-class breast tissue charac-
Fig. 6.2).

Studies in literature indicate that there has been remarkable interest amongst the research community to design computer-assisted classification systems for the prediction of breast density. These computer-aided classification systems are designed by using (a) segmented tissue approaches (STAs), or (b) fixed-size ROI approaches (ROIAs). It is worth mentioning that more studies have been carried out on
[29–39] and the related

[40–44]. It may be noted that computer-aided classification system designs using STAs require automatic segmentation of breast tissue that involves extra strides like taking out the background and expelling the pectoral muscle. Thus, STAs are more complex as well as time consuming in contrast with the ROIAs.

A brief explanation of work carried out on the DDSM database for 4-class clas-
Table 6.2.

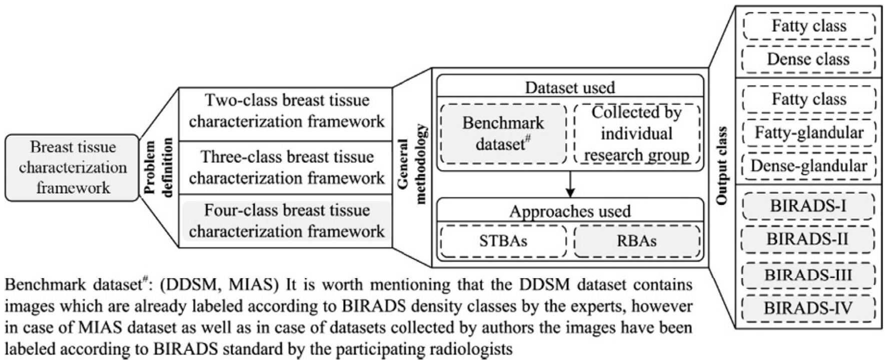

FIG. 6.2

Development of breast tissue characterization framework.

Table 6.2 Description of studies performed on the DDSM database for 4-class classification

Author (year)	STA/ROIA	No. of images	Classifier	Accuracy (%)
[31]	STA	377	NN	71.4
[32]	STA	615	*k*-NN	47.0
[34]	STA	500	SVM	84.7
[35]	STA	132	*k*-NN	77.0
[40]	ROIA	480	SVM	73.7
[41]	ROIA	480	HCF	84.6
[42]	ROIA	480	ANN	90.8
Present work	ROIA	480	ANN	92.1

The studies carried out in the past on DDSM dataset reports the maximum accuracy of 84.7% using STA and 90.8% using ROIA for 4-class breast tissue pattern characterization using GLCM-mean texture descriptors that have an ROI of fixed [42] [42], the author designed a breast density classifier system using assembly of six binary artificial neural network classifiers and obtained an accuracy of 90.8%. The present work is different from the [42] because the present work utilizes a computerized framework designed for 4-class breast tissue pattern characterization using the concept of weighted score fusion of ensemble neural network classifier, and the designed framework yields an accuracy of 92.1%.

The participating radiologist suggested that radiologists look for the center location of the mammographic images in the clinical environment (i.e., just behind

the nipple where the glandular ducts are present) as it contains the maximum density information, and it reflects sufficient information for identification of different classes of breast density. A similar observation also has been reported and exper-
[45]. Hence, in the present study, ROIs of a predefined size (128 × 128 pixels) are taken out from the central region of the breast in order to extract the accurate information regarding density class. Using GLCM statistical model $GLCM_{mean}$, feature vectors (TFVs) are extracted from each ROI, which gives the sufficient textural information to discriminate different breast tissue density patterns. To reduce the feature vector space, dimensionality principal component analysis algorithm is used, and reduced TFVs are directly fed to classification module for breast tissue density pattern class prediction.

Section 6.2 provides the detailed information about the materials and methods. This section also provides the detail description of used dataset, proposed methodology, ROI extraction, $GLCM_{mean}$ feature extraction, and classification module of the pro-
Section 6.3 consists of experiments, and their outcome is called
Section 6.4 provides the analysis of achieved results and comparison with
Section 6.5 is the conclusiotn of the work and provides the

6.2 Materials and methods

This work proposes a 4-class breast tissue pattern classification using the principal component analysis (PCA) and weighted score fusion of neural network classifiers. In this developed system, the radiologists are required to locate an ROI of size 128 × 128 pixels at the central portion of the breast where the presence of glandular ducts is significant. The desired features will be computed by the designed framework without human intervention, which will further pass the TFV through the classification module, and the density class of unknown ROI shall be predicted based on

6.2.1 Dataset description

In this work, 480 mammographic images consisting of 120 ϵ B1, 120 ϵ B2, 120 ϵ B3, and 120 ϵ B4 were taken from DDSM dataset. The DDSM dataset consists of a total
[46].
The depiction of the used dataset for the present work in terms of the total number of images, the number of extracted ROIs, and the bifurcation of data into training and
Fig. 6.3.

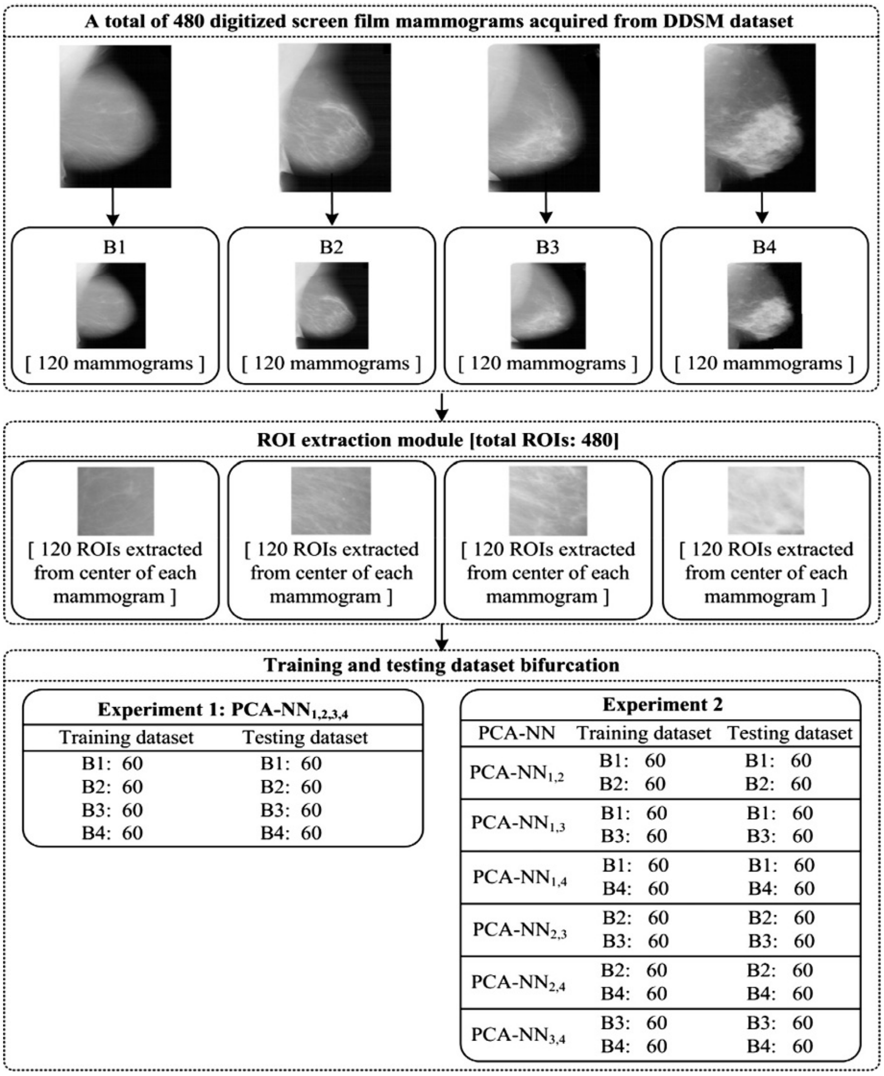

FIG. 6.3

Description of dataset and its bifurcations.

6.2.2 Experimental diagram for the designing of a breast tissue characterization framework using PCA and weighted score fusion of neural network classifiers

The experimental diagram for the designing of a breast tissue characterization frame-

Fig. 6.4.

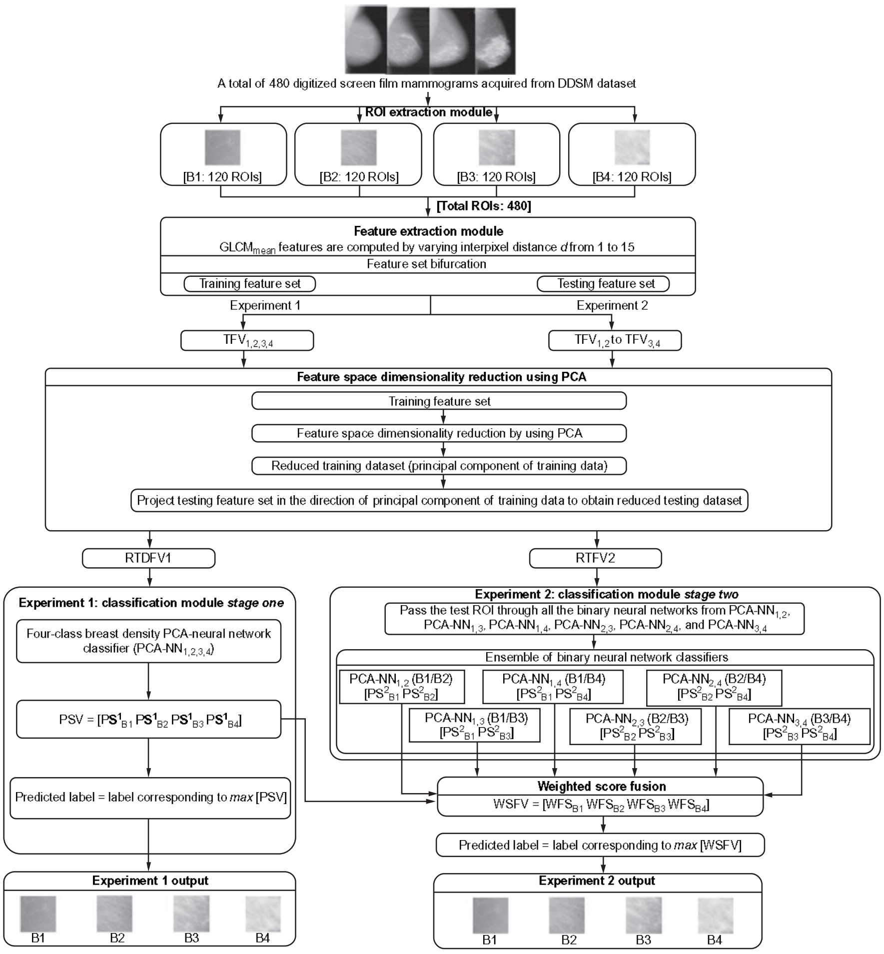

FIG. 6.4

Experimental diagram for designing a breast tissue pattern characterization framework using PCA and weighted score fusion of neural network classifiers. PS_{B1}, probability score value for B1 class; PS_{B2}, probability score value for B2 class; PS_{B3}, probability score value for B3 class; PS_{B4}, probability score value for B4 class; *WSFV*, weighted score fusion vector; WFS_{B1}, weighted fusion score value for B1 class; WFS_{B2}, weighted score fusion value for B2 class; WFS_{B3}, weighted score fusion value for B3 class; WFS_{B4}, weighted score fusion score value for B4 class.

6.2.3 ROI extraction module

[40–42,45], it has been observed that the central location of the breast reflects the highest information about density. Moreover it is also opined by the participating radiologist (also coauthor of this manuscript) that the central area of breast (i.e., just behind the

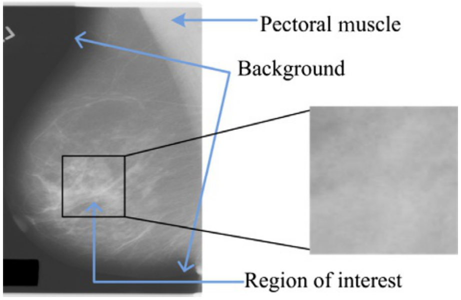

FIG. 6.5

ROI extraction module.

nipple) around the glandular ducts should be visualized for the purpose of discrimination between different breast tissue density pattern classes. Thus, for the designing of an efficient characterization framework, fixed size ROIs of 128×128 pixels are

Fig. 6.5

6.2.4 GLCM$_{\text{mean}}$ feature extraction

In the present study, the texture features are computed using gray level cooccurance

[14,41,42,47–52]. Using GLCM statistical model, GLCM$_{\text{mean}}$ features are extracted, which gives the sufficient textural information to discriminate different breast tissue density patterns. To calculate GLCM$_{\text{mean}}$ features, four directional GLCM features were obtained at first for each sample belonging to each of B1, B2, B3, and B4 class. The GLCM$_{\text{mean}}$ textural descriptor for a sample corresponding to a particular breast tissue pattern class is

(6.1).

$$\text{GLCM}_{\text{mean},\text{B1}(d=i)} = \frac{\text{GLCM}_{\text{B1}(0^\circ,d=i)} + \text{GLCM}_{\text{B1}\left(\frac{\Pi}{4},d=i\right)} + \text{GLCM}_{\text{B1}\left(\frac{\Pi}{2},d=i\right)} + \text{GLCM}_{\text{B1}\left(\frac{3\Pi}{4},d=i\right)}}{4} \quad (6.1)$$

Similarly, GLCM$_{\text{mean}}$ features for B2 class, i.e., GLCM$_{\text{mean,B2}(d=i)}$, GLCM$_{\text{mean}}$ features for B3 class, i.e., GLCM$_{\text{mean,B3}(d=i)}$ and GLCM$_{\text{mean}}$ features for B4 class, i.e., GLCM$_{\text{mean,B4}(d=i)}$ are determined by varying d i.e. $\{d \in [1, 2, \ldots, 15]\}$, where d is known as interpixel distance.

The GLCM$_{\text{mean}}$ features obtained at an interpixel distance $d=10$ for ROI images that belongs to B1, B2, B3, and B4 breast tissue pattern classes have been mapped as

Fig. 6.6A–D, respectively.

Fig. 6.6 that GLCM$_{\text{mean}}$ plot is comparatively less dispersed for B1 class ROIs, and this dispersion appears to be increasing as we move from B1 to B4 class ROIs. On observing GLCM$_{\text{mean}}$ elements plots for the testing

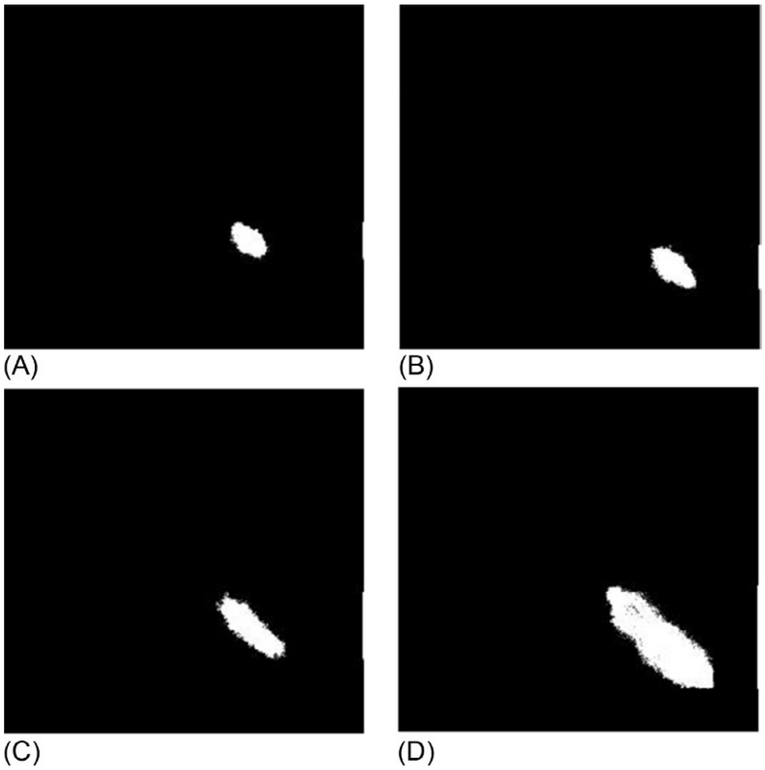

FIG. 6.6

$GLCM_{mean}$ elements of four directions (for $\theta = 0°$, $\pi/4$, $\pi/2$ and $3\pi/4$). (A) B1 ROI: A_1943_1.LMLO, (B) B2 ROI: B_3366_1.RMLO, (C) B3 ROI: C_0243_1.RMLO, and (D) B4 ROI: B_3175_1.RMLO. *LMLO,* left MLO; *RMLO,* right MLO.

instance that belongs to BIRADS breast tissue pattern class, it can be concluded that it reflects considerable information regarding variations in texture patterns that play a very important role for classification between various breast tissue patterns.

The value of $GLCM_{mean}$ feature for angular second moment (ASM) is computed at $d=$ (6.2).

$$ASM_{mean(d=10)} = \left(\frac{ASM_{(\theta=0°, d=10)} + ASM_{(\theta=\Pi/4, d=10)} + ASM_{(\theta=\Pi/2, d=10)} + ASM_{(\theta=3\Pi/4, d=10)}}{4} \right) \quad (6.2)$$

In a similar way, the rest of the $GLCM_{mean}$ texture features ($contrast_{mean}$, $variance_{mean}$, inverse difference $moment_{mean}$, $correlation_{mean}$, sum $average_{mean}$, sum $variance_{mean}$, difference $variance_{mean}$, $entropy_{mean}$, sum $entropy_{mean}$, difference $entropy_{mean}$, information measures of correlation-1_{mean}, information

Table 6.3 Extracted TFVs used for designing used classifiers

Experiment	TFVs	*l*	Description of TFVs used classifier designing
Experiment 1	$TFV_{1,2,3,4}$	13	TFV subjected to PCA for design of $PCA\text{-}NN_{1,2,3,4}$ classifier
Experiment 2	$TFV_{1,2}$	13	TFV used for designing binary $PCA\text{-}NN_{1,2}$ classifier
	$TFV_{1,3}$	13	TFV used for designing binary $PCA\text{-}NN_{1,3}$ classifier
	$TFV_{1,4}$	13	TFV used for designing binaryPCA-$NN_{1,4}$ classifier
	$TFV_{2,3}$	13	TFV used for designing binary $PCA\text{-}NN_{2,3}$ classifier
	$TFV_{2,4}$	13	TFV used for designing binary $PCA\text{-}NN_{2,4}$ classifier
	$TFV_{3,4}$	13	TFV used for designing binary $PCA\text{-}NN_{3,4}$ classifier

TFVs, *texture feature vectors;* l, *length of TFVs.*

measures of correlation-2_{mean}) are calculated for interpixel distance (d) varying from 1 to 15. It has been observed that the TFV extracted at $d=10$ yields the highest classification accuracy of 79.6%. Thus, it can be concluded that the $GLCM_{mean}$ features computed at an interpixel distance $d=10$, yields maximum information for differential diagnosis between different breast tissue density patterns. Thus, all the $GLCM_{mean}$ TFVs were computed at $d=10$. The brief description of these Table 6.3.

6.2.5 Feature space dimensionality reduction stage

The performance of the designed system sometimes degrades due to the presence of redundant features. So feature space dimensionality reduction stage using PCA is [53,54]. The steps of Fig. 6.7.

The optimal length of these reduced texture feature vectors (RTFVs), i.e., the optimal number of PCs for designing a particular neural network classifier has been decided based on exhaustive experiments carried out by varying the PCs from 2 to 10 in steps of 1. To get the optimal values of PCs for characterization between different breast tissue pattern, RTFVs have been computed for all the seven neural networks, i.e., for single 4-class $PCA\text{-}NN_{1,2,3,4}$ (B1/B2/B3/B4) and collection of six binary PCA neural network classifiers, i.e., $PCA\text{-}NN_{1,2}$ (B1/B2), $PCA\text{-}NN_{1,3}$ (B1/B3), $PCA\text{-}NN_{1,4}$ (B1/B4), $PCA\text{-}NN_{2,3}$ (B2/B3), $PCA\text{-}NN_{2,4}$ (B2/B4), and $PCA\text{-}NN_{3,4}$ (B3/B4). The optimal length of these RTFVs for all the neural network designs with Table 6.4

6.2.6 Classification module

The classification module in the CAD system design is used to predict the class identification of unknown instances based on the class information of the instances present in the training dataset. For the classification of analysis and classification of

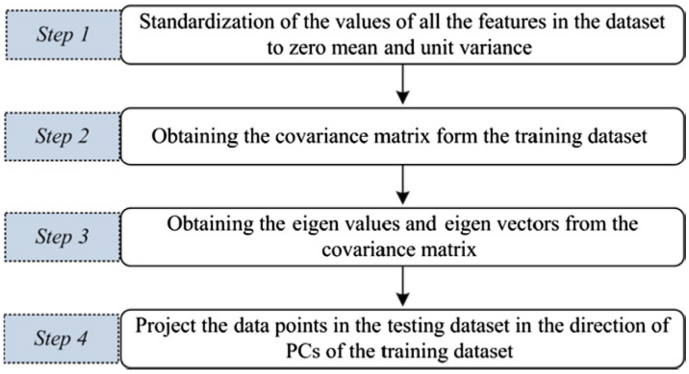

FIG. 6.7

Steps of PCA algorithm.

Table 6.4 Optimal number of principal components and hidden layers with highest prediction rate for each ANN using RTFVs

Classification stage	RTFVs	Neural network [(classes), (I:H:O)]	RTFVs description	*pc* (l)	Accuracy (%)
Stage one	RTFV1	PCA-$NN_{1,2,3,4}$ [(B1/B2/B3/B4), (13:7:4)]	$RTFV_{1,2,3,4}$	9	79.6
Stage two	RTFV2	PCA-$NN_{1,2}$ [(B1/B2), 13:5:2]	$RTFV_{1,2}$	8	94.1
		PCA-$NN_{1,3}$ [(B1/B3), 13:6:2]	$RTFV_{1,3}$	9	95.8
		PCA-$NN_{1,4}$ [(B1/B4), 13:4:2]	$RTFV_{1,4}$	5	100
		PCA-$NN_{2,3}$ [(B2/B3), 13:6:2]	$RTFV_{2,3}$	9	82.5
		PCA-$NN_{2,4}$ [(B2/B4), 13:5:2]	$RTFV_{2,4}$	7	98.3
		PCA-$NN_{3,4}$ [(B3/B4), 13:5:2]	$RTFV_{3,4}$	8	89.1

RTFVs, *reduced TFVs;* l, *length of reduced RTFVs;* pc, *optimum number of principal components (number of eigen features);* I, *input layer neurons;* H, *hidden layer neurons;* O, *output layer neurons.*

medical images, various classifiers have been employed in the past, popular choice being *k*- [32,35,55–57] [14,55,57] [14,34,40,55,57,58] [31,54–57,59–64]. A brief description of each classifier is given as:

(1) *k-NN classifier*: Based on the concept of majority voting, this classifier estimates the class of an unknown instance based on the class of its *k* nearest neighbors in the training dataset. The nearest neighbors are estimated based on the distance metric. Different types of distance metrics like Euclidean, Cosine, [55–58].

(2) *PNN classifier*: A supervised feed-forward neural network used for estimating the probability of class membership of the unknown instance. The architecture of PNN consists of four layers: input layer, pattern layer, summation layer, and [14,55,57,58].

(3) *SVM classifier*: Based on the concept of hyperplanes that are used to separate the instances of the two classes clearly. SVM classifier can be used for both linearly and nonlinearly separable data. The nonlinear data problem can be converted into a linear one with the help of kernel functions that map the nonlinear data from the input space to a linearly separable data in the higher dimensional output [14,55,57,58].

(4) *NN classifier* Fig. 6.8. The NN consists of input layer, hidden layer, summation layer, and output layer. Input layer is used for taking input as a feature vector of testing image, and output layer is used to provide the output class information on the basis of probability score value [42,55–57].

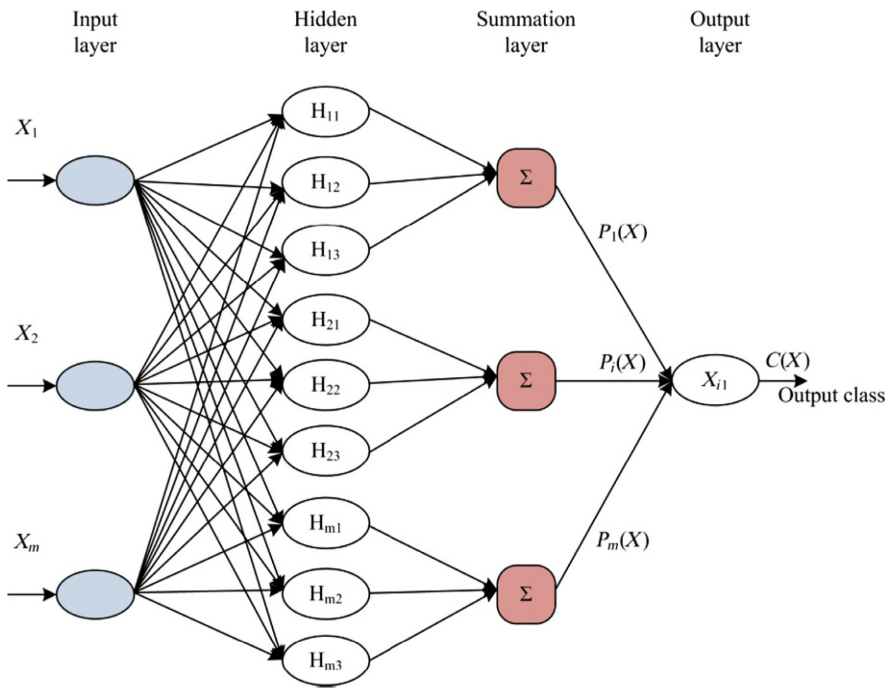

FIG. 6.8

Architecture of neural network classifier. $X_{1,2,\ldots,m}$, input feature vector; $P_i(X)$, probability score for X class of ROI; *H*, hidden layer.

In the present work, NN classifier has been used for characterization between different breast tissue density patterns.

The developed characterization framework is comprised of two stages: (i) *Stage one*: A single 4-class PCA-$NN_{1,2,3,4}$ classifier, i.e., PCA-$NN_{1,2,3,4}$ (B1/B2/B3/B4). (ii) *Stage two*: An assembly of binary PCA-neural network classifiers for each pair of classes, i.e., PCA-$NN_{1,2}$ (B1/B2), PCA-$NN_{1,3}$ (B1/B3), PCA-$NN_{1,4}$ (B1/B4), PCA-$NN_{2,3}$ (B2/B3), PCA-$NN_{2,4}$ (B2/B4), and PCA-$NN_{3,4}$ (B3/B4) for classification between individual BIRADS classes.

The description of each classification stage, i.e., *Stage one* and *Stage two* is Fig. 6.9.

6.2.6.1 Classification module: Stage one

This stage includes a 4-class PCA-NN classifier, i.e., PCA-$NN_{1,2,3,4}$ i.e. B1/B2/B3/B4, which yields the probability score vector (PSV = [$\mathbf{PS}^1_{B1}$ $\mathbf{PS}^1_{B2}$ $\mathbf{PS}^1_{B3}$ $\mathbf{PS}^1_{B4}$]) and indicates the probability score through which a test ROI corresponds to a specific class of breast tissue pattern.

In order to obtain the optimal training model for PCA-$NN_{1,2,3,4}$ the model is trained repeatedly and validated using $GLCM_{mean}$ TFVs ($TFV_{1,2,3,4}$) computed at d from 1 to 15 and by varying length of principal component pc from 1 to 10. The highest accuracy of 79.6% is attained by using $GLCM_{mean}$ features ($RTFV_{1,2,3,4}$) computed at an interpixel distance d ($d=10$), and the length of principal component is $pc=9$.

6.2.6.2 Classification module: Stage two

This stage includes a collection of six binary PCA-NN classifiers, i.e., PCA-$NN_{1,2}$ (B1/B2), PCA-$NN_{1,3}$ (B1/B3), PCA-$NN_{1,4}$ (B1/B4), PCA-$NN_{2,3}$ (B2/B3), PCA-$NN_{2,4}$ (B2/B4), and PCA-$NN_{3,4}$ (B3/B4) for classification between individual BIRADS classes, which yields weighted fusion score values (WFSV).

The probability score obtained from the *stage one* of breast tissue characterization framework, i.e., output of PCA-$NN_{1,2,3,4}$ is utilized in order to obtain the most likely breast tissue pattern classes for an input test ROI using the obtained probability score values [$\mathbf{PS}^2_{B1}$ $\mathbf{PS}^2_{B2}$ $\mathbf{PS}^2_{B3}$ $\mathbf{PS}^2_{B4}$] for an input test ROI. In case of *stage two*, the test ROI is preceded to all six binary PCA-NN classifiers, which yields weighted fusion score vector (WFSV). The class corresponding to the maximum weighted fusion score vector (WFSV) corresponding to the predicted class label of the test [59].

In general, if fusion score vector (WFS_{uv}) is the output from ensemble of six binary neural network classifiers between u and v class corresponding to class u for input RTFVs, then weighted fusion score vector ($WFSV_u$) for class u is defined (6.3).

$$WFSV_u = PS_u \times \sum_{v=1, v\neq u}^{4} WFS_{uv}(RTFV), \quad \forall_{ij} \in \{B1, B2, B3, B4\} \tag{6.3}$$

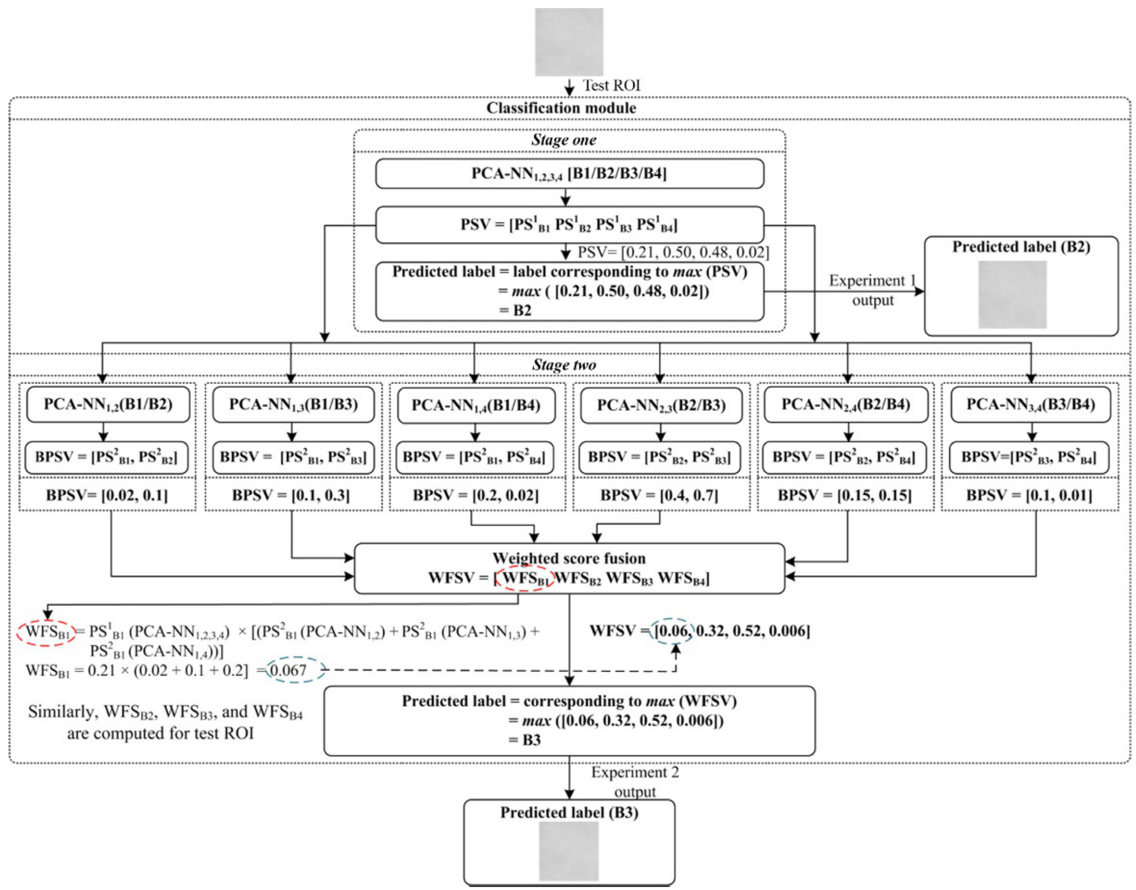

FIG. 6.9

Flow diagram of the classification module. *PSV*, probability score vector; *BPSV*, binary PSV; *WFSV*, weighted fusion score vector; *WFS*, weighted fusion score. Example of a test ROI i.e. misclassified by *stage one* and correctly classified by *stage two*.

(6.3), and the class corresponding to the maximum fusion score value (WFS) is the to the predicted class label for the test ROI.

For designing PCA-$NN_{1,2,3,4}$ and six binary PCA-NN neural network classifiers, i.e., PCA-$NN_{1,2}$ (B1/B2), PCA-$NN_{1,3}$ (B1/B3), PCA-$NN_{1,4}$ (B1/B4), PCA-$NN_{2,3}$ (B2/B3), PCA-$NN_{2,4}$ (B2/B4), and PCA-$NN_{3,4}$ (B3/B4) adaptive learning with back propagation is utilized. For obtaining the optimal number of neurons for the hidden

[37,50–54,59]. After exhaustive experiments, the obtained optimum number of hidden layers for every PCA-NN design

Table 6.4.

The task executed in classification module *stage one* (i.e., processing an input test ROI through PCA-$NN_{1,2,3,4}$) is similar to showcasing the testing sample to a radiologist having the expertise in differentiating between the 4-class breast tissue density pattern where the radiologist provides the probability score value to predict the corresponding class of an input test ROI. Assuming that the participating radiologist predicts a probability score value [$\mathbf{PS}^1_{B1}$ (0.21) $\mathbf{PS}^1_{B2}$ (0.50) $\mathbf{PS}^1_{B3}$ (0.48) $\mathbf{PS}^1_{B4}$ (0.02)] for an input test ROI. In *stage one*, the label of input test ROI is predicted as the maximum probability score value for an input test. ROI is class label, i.e., max ([$\mathbf{PS}^1_{B1}$ (0.21) $\mathbf{PS}^1_{B2}$ (0.50) $\mathbf{PS}^1_{B3}$ (0.48) $\mathbf{PS}^1_{B4}$ (0.02)]) = $\mathbf{PS}^1_{B2}$ (0.50) is predicted to the input test ROI, therefore predicted class label is B2.

The work performed in classification module *stage two* (i.e., passing the input test ROI through all binary PCA-NN neural networks, i.e., PCA-$NN_{1,2}$, PCA-$NN_{1,3}$, PCA-$NN_{1,4}$, PCA-$NN_{2,3}$, PCA-$NN_{2,4}$, and PCA-$NN_{3,4}$) is reconsulting from six experienced radiologists who have expertise in making differential diagnosis between (B1/B2), (B1/B3), (B1/B4), (B2/B3), (B2/B4), and (B3/B4) breast density classes respectively. Every binary neural network predicts the same probability score for test ROI, and these predicted probability scores are fused together, resulting

(6.3). The probability score value for test ROI from PCA-$NN_{1,2}$: [$\mathbf{PS}^2_{B1}$ (0.02) $\mathbf{PS}^2_{B2}$ (0.1)], PCA-$NN_{1,3}$: [$\mathbf{PS}^2_{B1}$ (0.1) $\mathbf{PS}^2_{B3}$ (0.3)], PCA-$NN_{1,4}$: [$\mathbf{PS}^2_{B1}$ (0.2) $\mathbf{PS}^2_{B4}$ (0.02)], PCA-$NN_{2,3}$: [$\mathbf{PS}^2_{B2}$ (0.4) $\mathbf{PS}^2_{B3}$ (0.7)], PCA-$NN_{2,4}$: [$\mathbf{PS}^2_{B2}$ (0.15) $\mathbf{PS}^2_{B4}$ (0.15)], and PCA-$NN_{3,4}$: [$\mathbf{PS}^2_{B3}$ (0.1) $\mathbf{PS}^2_{B4}$ (0.01)]. After imple-

(6.3), the WFSV for the test ROI is [WFS_{B1} WFS_{B2} WFS_{B3} WFS_{B4}]: [0.06, 0.32, 0.52, 0.006]. The class label for this test ROI is predicted by maximum of WFSV i.e., *max* ([0.06, 0.32, 0.52, 0.006]) = WFS_{B3} (0.52) is predicted to the input

6.3 Experiments and analysis of results

The exhaustive experiments have been conducted for the designing of a breast tissue pattern characterization framework using principal component analysis and weighted score fusion of neural network classifiers. The list of experiments carried

Table 6.5.

Table 6.5 List of experiments carried out in this work

Experiment no.	Description
Experiment no. 1	Breast tissue characterization framework using PCA-$NN_{1,2,3,4}$ classifier (classification module: *stage one*)
Experiment no. 2	Breast tissue characterization framework using six binary neural network classifiers (classification module: *stage two*)

6.3.1 Experiment 1

The classification accuracy of RTFV1 ($GLCM_{mean}$ texture feature vector obtained at interpixel distance d i.e. $d=10$ and principal component number pc i.e. $pc=9$) for 4-class breast tissue pattern classes is tested using PCA-$NN_{1,2,3,4}$ Table 6.6 shows the summary of obtained results (i.e., accuracies obtained by the *stage one*).

Table 6.6, it can be concluded that PCA-$NN_{1,2,3,4}$ capitulate 79.6% (191/240) as overall classification accuracy (i.e., 191 testing ROIs have been classified into correct class from 240 testing ROIs). The correctly classified ROIs 191 (191/240) consist of 52 (52/60) B1, 50 (50/60) B2, 32 (32/60) B3, and 57 (57/60) B4 cases. Hence, the value of individual class accuracy (ICA) 86.6% (52/60), 83.3% (50/60), 53.3% (32/60), and 95.0% (57/60) are obtained for B1, B2, B3, and B4 classes respectively.

The results obtained at stage one, i.e., PCA-$NN_{1,2,3,4}$ is graphically demonstrated Fig. 6.10

6.3.2 Experiment 2

The obtained performance of RTFV2 ($RTFV_{1,2}$ to $RTFV_{3,4}$) for $GLCM_{mean}$ features at interpixel distance $d=10$ for characterization between 4 class breast tissue

Table 6.6 Results obtained by the classification module *stage one*, i.e., PCA-$NN_{1,2,3,4}$

		CM				
		Predicted class label				
		B1	B2	B3	B4	ICA (%)
Ground truth class	B1	52	6	1	1	86.6
	B2	3	50	6	1	83.3
	B3	0	12	32	16	53.3
	B4	0	0	3	57	95.0
Overall classification accuracy (%)						79.6

CM, *confusion matrix;* ICA, *individual class accuracy.*

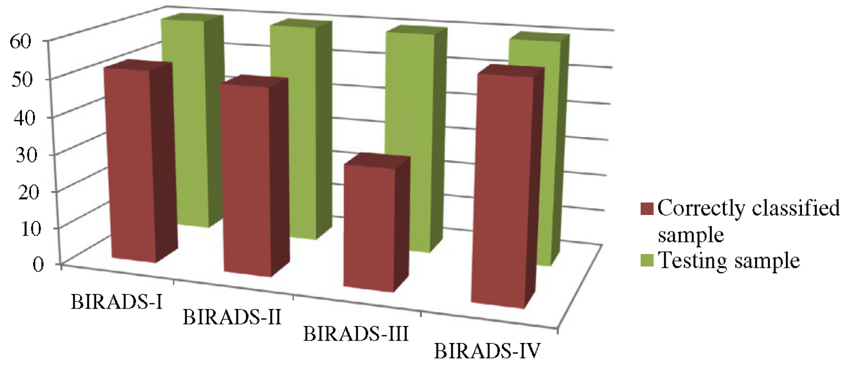

FIG. 6.10

Results obtained by PCA-$NN_{1,2,3,4}$.

Table 6.7 Results obtained by the classification module *stage two*

		CM				
		Ground truth class				
		B1	**B2**	**B3**	**B4**	**ICA**
Predicted class label	B1	58	2	0	0	96.6
	B2	1	55	2	2	91.6
	B3	0	3	48	9	80.0
	B4	0	0	0	60	100
Overall classification accuracy						92.1

CM, *confusion matrix;* ICA, *individual class accuracy.*

pattern classes is validated using a collection of six binary PCA-NN classifiers. The performance yielded by the *stage two*
Table 6.7.

The results obtained from the execution of *stage two* Table 6.7) of classification module, i.e., PCA-$NN_{1,2}$ (B1/B2), PCA-$NN_{1,3}$ (B1/B3), PCA-$NN_{1,4}$ (B1/B4), PCA-$NN_{2,3}$ (B2/B3), PCA-$NN_{2,4}$ (B2/B4), and PCA-$NN_{3,4}$ (B3/B4) shows the OCA value of 92.1% (i.e., a total of 221 testing ROIs have been correctly classified into correct class from 240 testing ROIs). A total of 221 correctly classified ROIs comprised of 58 (58/60) B1 class, 55 (55/60) B2 class, 48 (48/60), B3 class, and 60 (60/60) B4 class. Hence, the ICA values of 96.6% (58/60), 91.6% (55/60), 80.0% (48/60), and 100% (60/60) are achieved for B1 class, B2 class, B3 class, and B4 class, respectively.

The obtained performance of RTFV2 ($RTFV_{1,2}$ to $RTFV_{3,4}$) for $GLCM_{mean}$ features at interpixel distance $d=$ Fig. 6.11.

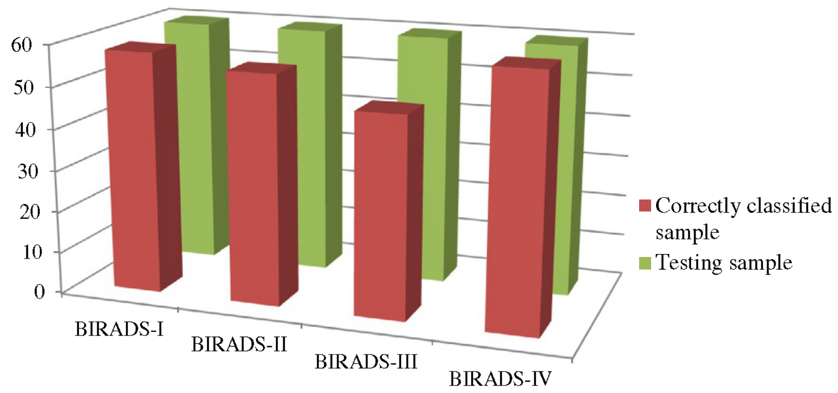

FIG. 6.11

Results obtained for RTFV2 ($RTFV_{1,2}$ to $RTFV_{3,4}$) using $GLCM_{mean}$ features.

6.4

6.4.1 Misclassification analysis

In case of misclassification analysis, it has been found that only 19 testing samples are misclassified at *stage two* of the classification module while 49 testing samples are misclassified at *stage one* of the classification module out of a total of 240 testing samples.

The brief description of misclassification analysis at each classification stage is Table 6.8.

The 19 out of 240 testing samples are misclassified, which comprised of 2 (2/60) misclassified samples belongs to B1 class, 5 (5/60) belongs to B2 class, 12 (12/ 60) belongs to B3 class and nil (0/60) belongs to B4 class respectively.

Table 6.8 that a majority of misclassified cases belong to the B2 or B3 breast tissue pattern classes. A total of 30 ({6 ϵ B1} + {5 ϵ B2} +

Table 6.8 Description of misclassification for each stage

Testing sample	Misclassification at *stage one*	Misclassification at *stage two*
{60 ϵ B1} {60 ϵ B2} {60 ϵ B3} {60 ϵ B4}	{08 ϵ B1} {10 ϵ B2} {28 ϵ B3} {03 ϵ B4}	{02 ϵ B1} {05 ϵ B2} {12 ϵ B3} {00 ϵ B4}
Total: 240	Total: 49	Total: 19

Note: *Total 30 (49–19) testing samples misclassified by* stage one *are correctly classified by* stage two.

{16 ϵ B3}+{3 ϵ B4}) samples that are incorrectly classified by *stage one* have been correctly classified after passing all testing samples to *stage two*. However, 16 incorrectly classified ROIs belonging to B3 class, 5 incorrectly classified ROIs belonging to B2 class, 6 incorrectly classified ROIs belonging to B1 class, and 3 incorrectly classified ROIs belonging to B4 class have been classified into correct breast tissue pattern class after passing through *stage two* of classification module. The remaining 19 testing ROIs have been incorrectly classified, and can be correctly classified after inclusion of next higher level of classification

6.4.2 Comparative analysis

From the results of experiment 1 and experiment 2, it has been observed that the number of incorrectly classified instances have lessened from 49 (49/240) to 19 (19/240) after the inclusion of *stage two*; resulting n improvement in total classification accuracy from 79.6% to 92.1%, and the ICA values for B1, B2, B3, and B4 have increased by 10%, 8.3%, 26.7%, and 6.7% respectively. It also can be observed that the all the cases belonging to extremely dense, i.e., B4 class has been correctly classified after passing the testing instances to *stage two* of classification module.

The proposed classification framework is compared with the study performed by [42]
Table 6.9. The parameters based on classification accuracy, i.e., OCA values: ICA_{B1}, ICA_{B2}, ICA_{B3}, ICA_{B4} and statistical analysis using Cohen's kappa method is used for the comparative analysis.
[65] has been performed for both classification framework, and it was found that the proposed classification framework is more reliable and recommended for clinical environment for breast density classification.

Table 6.9 Comparative analysis for proposed and study carried out by Kumar [42]

Designed framework	Accuracy (%)					Cohen's kappa value
	OCA	ICA_{B1}	ICA_{B2}	ICA_{B3}	ICA_{B4}	
[42]	90.8	98.3	91.6	80.0	93.3	0.877
Proposed	92.1	96.6	91.6	80.0	100	0.894

ICA_{B1}, *individual class accuracy for B1;* ICA_{B2}, *individual class accuracy for B2;* ICA_{B3}, *individual class accuracy for B3;* ICA_{B4}, *individual class classification accuracy for B4.*

6.5 Conclusion

The study carried out in this work for breast tissue characterization into 4-class shows that the $GLCM_{mean}$ texture feature plays an important role in accounting for textural variations exhibited by different breast tissue density patterns. In daily clinical practice, there are so many cases where the breast tissue pattern class cannot be visually determined on the basis of subjective analysis, so the computerized frameworks for breast tissue pattern characterization come into play. In the clinical condition, it is a primary concern for a radiologist to effectively distinguish breast tissue pattern class. After that twofold check, the mammogram demonstrating a high breast tissue pattern should be searched for any lesions that may be holed up behind the dense tissue. By the help of computerized frameworks for breast tissue pattern characterization, vulnerabilities that are available at the time of visual examination can be evacuated. This also advances the demonstrative exactness by highlighting certain regions of doubt that may contain any tumors masked behind the dense tissue.

Conflicts of interest

None.

References

J. Ferlay, E. Foucher, J. Tieulent, S. Rosso, J.W. Coebergh, H. Comber, D. Forman, F. Bray, Cancer incidence and mortality patterns in Europe: estimates for 40 countries in 2012, Eur. J. Cancer 49 (2013) 1374–1403.

N.F. Boyd, H. Guo, L.J. Martin, L. Sun, J. Stone, E. Fishell, M.J. Yaffe, Mammographic density and the risk and detection of breast cancer, N. Engl. J. Med. 356 (2007) 227–236.

N.F. Boyd, G.A. Lockwood, J.W. Byng, D.L. Tritchler, M.J. Yaffe, Mammographic densities and breast cancer risk, Cancer Epidemiol. Biomarkers Prev. 7 (2008) 1133–1144.

N.F. Boyd, L. Martin, S. Chavez, A. Gunasekara, A. Salleh, A. Bronskill, Breast-tissue composition and other risk factors for breast cancer in young women: a cross-sectional study, Lancet Oncol. 10 (2009) 569–580.

N.F. Boyd, L.J. Martin, M.J. Yaffe, S. Minkin, Mammographic density and breast cancer risk: current understanding and future prospects, Breast Cancer Res. 13 (2011) 223–234.

N.F. Boyd, J.M. Rommens, K. Vogt, V. Lee, J.l. Hopper, M.J. Yaffe, A.D. Paterson, Mammographic breast density as an intermediate phenotype for breast cancer, Lancet Oncol. 6 (2005) 798–808.

C. Colin, V. Prince, P.J. Valette, Can mammographic assessments lead to consider density as a risk factor for breast cancer? Eur. J. Radiol. 82 (2013) 404–411.

A. Eng, Z. Gallant, J. Shepherd, V. McCormack, J. Li, M. Dowsett, I. dos-Santos-Silva, Digital mammographic density and breast cancer risk: a case-control study of six alternative density assessment methods, Breast Cancer Res. 16 (2014) 439–451.

C.M. Vachon, C.H. Van-Gils, T.A. Sellers, K. Ghosh, S. Pruthi, K.R. Brandt, S. Pankratz, Mammographic density, breast cancer risk and risk prediction, Breast Cancer Res. 9 (2007) 1–9.

J.N. Wolfe, Risk for breast cancer development determined by mammographic parenchymal pattern, Cancer 37 (1976) 2486–2492.

J.N. Wolfe, Breast patterns as an index of risk for developing breast cancer, Am. J. Roentgenol. 126 (1976) 1130–1137.

K. Ganesan, U. Acharya, C.K. Chua, L.C. Min, K.T. Abraham, K.B. Ng, Computer-aided breast cancer detection using mammograms: a review, IEEE Rev. Biomed. Eng. 6 (2013) 77–98.

S. Cheriguene, N. Azizi, N. Zemmal, N. Dey, H. Djellali, N. Farah, Optimized tumor breast cancer classification using combining random subspace and static classifiers selection paradigms, in: Applications of Intelligent Optimization in Biology and Medicine, Springer, Cham, 2016, pp. 289–307.

Kriti, J. Virmani, N. Dey, V. Kumar, PCA-PNN and PCA-SVM based CAD systems for breast density classification, in: Applications of Intelligent Optimization in Biology and Medicine, Springer, Cham, 2016, pp. 159–180.

N. Zemmal, N. Azizi, N. Dey, M. Sellami, Adaptive semi supervised support vector machine semi supervised learning with features cooperation for breast cancer classification, J. Med. Imaging Health Inform. 6 (1) (2016) 53–62.

N. Zemmal, N. Azizi, N. Dey, M. Sellami, Adaptative S3VM semi supervised learning with features cooperation for breast cancer classification, J. Med. Imaging Health Inform. 6 (4) (2016) 957–967.

L. Saba, N. Dey, A.S. Ashour, S. Samanta, S.S. Nath, S. Chakraborty, … J.S. Suri, Automated stratification of liver disease in ultrasound: an online accurate feature classification paradigm, Comput. Methods Prog. Biomed. 130 (2016) 118–134.

I. Kumar, J. Virmani, H.S. Bhadauria, A review of breast density classification methods, in: Proceeding of 2nd International Conference on Computing for Sustainable Global Development 'INDIACom—2015, 2015, pp. 1960–1967.

G. Zhang, W. Wang, J. Moon, J.K. Pack, S. Jean, A review of breast tissue classification in mammograms, in: Proceedings of ACM Symposium on Research in Applied Computation, 2011, pp. 232–237.

E.A. Abdel-Gawad, O.A. Khalil, S.M. Ragaee, Assessment of breast lesions using BI-RADS US lexicon in mammographically dense breasts (ACR categories 3 and 4) with histopathological correlation, Egypt. J. Radiol. Nucl. Med. 45 (2014) 1301–1307.

M. John, K. Karen, S. Carol, J. Seibert, A breast density index for digital mammograms based on radiologists ranking, J. Digit. Imaging 2 (1998) 101–115.

A. Tagliafico, G. Tagliafico, S. Tosto, F. Chiesa, C. Martinoli, L.E. Derchi, M. Calabrese, Mammographic density estimation: comparison among BI-RADS categories, a semi-automated software and a fully automated one, Breast 18 (2009) 35–40.

R. Pereira, P.M. Marques, O.M. Honda, S.K. Kinoshita, R. Engelmann, C. Muramatsu, K. Doi, Usefulness of texture analysis for computerized classification of breast lesions on mammograms, J. Digit. Imaging 20 (2007) 248–255.

A. Oliver, M. Tortajada, X. Llado, J. Freixenet, S. Ganau, L. Tortajada, R. Marti, Breast density analysis using an automatic density segmentation algorithm, J. Digit. Imaging 28 (2015) 604–612.

A. Papaevangelou, S. Chatzistergos, K.S. Nikita, G. Zografos, Breast density: computerized analysis on digitized mammograms, Hell. J. Surg. 83 (2011) 133–138.

J.J. Heine, M.J. Carton, C.G. Scott, An automated approach for estimation of breast density, Cancer Epidemiol. Biomarkers Prev. 17 (2008) 3090–3097.

Z. Huo, M.L. Giger, C.J. Vyborny, Computerized analysis of multiple-mammographic views: potential usefulness of special view mammograms in computer-aided diagnosis, IEEE Trans. Med. Imaging 20 (2001) 1285–1292.

L. Yaghjyan, S. Pinney, M. Mahoney, A. Morton, J. Buckholz, Mammographic breast density assessment: a methods study, Atlas J. Med. Biol. Sci. 1 (2011) 8–14.

P. Miller, S. Astley, Classification of breast tissue by texture analysis, in: Proceeding of BMVC91, 1991, pp. 258–265.

N. Karssemeijer, Automated classification of parenchymal patterns in mammograms, Phys. Med. Biol. 43 (1998) 365–369.

K. Bovis, S. Singh, Classification of mammographic breast density using a combined classifier paradigm, in: Proceeding of 4th International Workshop on Digital Mammography, 2002, pp. 177–180.

A. Oliver, J. Freixenet, R. Zwiggelaar, Automatic classification of breast density, in: Proceedings of the IEEE International Conference on Image Processing 'ICIP 2005' Genova, 2005, pp. 1258–1261.

N. Jamal, K.H. Ng, S. Ranganathan, L.K. Tan, Comparison of computerized assessment of breast density with subjective BI-RADS classification and Tabar's pattern from two-view CR mammography, in: Proceeding of World Congress on Medical Physics and Biomedical Engineering, 2006, pp. 1405–1408.

A. Bosch, X. Munoz, A. Oliver, J. Marti, Modeling and classifying breast tissue density in mammograms, in: Proceeding of Computer Vision and Pattern Recognition, 2006, pp. 1552–1558.

A. Oliver, J. Freixenet, R. Marti, J. Pont, E. Perez, E.R. Denton, R. Zwiggelaar, A novel breast tissue density classification methodology, IEEE Trans. Inf. Technol. B 12 (2008) 55–65.

Y. Qu, C. Shang, W. Wu, Q. Shen, Evolutionary fuzzy extreme learning machine for mammographic risk analysis, Int. J. Fuzzy Syst. 13 (2011) 282–291.

Z. Chen, E. Denton, R. Zwiggelaar, Local feature based mammographic tissue pattern modeling and breast density classification, in: Proceeding of 4th International Conference on Biomedical Engineering and Informatics, 2011, pp. 351–355.

A.D. Masmoudi, N.G.B. Ayed, D.S. Masmoudi, A. Abid, LBPV descriptors-based automatic ACR/BIRADS classification approach, J. Image Video Process. 1 (2013) 1–9.

W. He, S. Harvey, A. Juette, E. Denton, R. Zwiggelaar, Mammographic segmentation and density classification: a fractal inspired approach, in: Proceeding of International Workshop on Digital Mammography, 2016, pp. 359–366.

I. Kumar, J. Virmani, H.S. Bhadauria, Wavelet packet texture descriptors based four-class BIRADS breast tissue density classification, Procedia Comput. Sci. 70 (2015) 76–84.

I. Kumar, H.S. Bhadauria, J. Virmani, S. Thakur, A hybrid hierarchical framework for classification of breast density using digitized film screen mammograms, Multimed. Tools Appl. 76 (18) (2017) 1–25.

I. Kumar, H.S. Bhadauria, J. Virmani, S. Thakur, A classification framework for prediction of breast density using an ensemble of neural network classifiers, Biocybern. Biomed. Eng. 37 (2017) 217–228.

M. Mustra, M. Grgic, K. Delac, Breast density classification using multiple feature selection, Autom. J. Control Meas. Electron. Comput. Commun. 53 (2012) 362–372.

Q. Liu, L. Liu, Y. Tan, J. Wang, X. Ma, X. Ni, Mammogram density estimation using sub-region classification, in: Proceeding of 4th International Conference on Biomedical Engineering and Informatics, 2011, pp. 356–359.
H. Li, M.L. Giger, Z. Huo, O.I. Olopade, L. Lan, B.L. Weber, I. Bonta, Computerized analysis of mammographic parenchymal patterns for assessing breast cancer risk: effect of ROI size and location, Med. Phys. 31 (2004) 549–555.
M. Heath, K. Bowyer, D. Kopans, V. Moore, W.P. Kegelmeyer, The digital database for screening mammography, in: Proceedings of the 5th International Workshop on Digital Mammography, 2000, pp. 212–221.
R.M. Haralick, K. Shanmugam, J.H. Dinstein, Textural features for image classification, IEEE Trans. Syst. Man. Cyb. 6 (1973) 610–621.
H. Li, M.L. Giger, O.I. Olopade, A. Margolis, L. Lan, M.R. Chinander, Computerized texture analysis of mammographic parenchymal patterns of digitized mammograms, Acad. Radiol. 12 (2005) 863–873.
J.S. Weszka, C.R. Dyer, A. Rosenfeld, A comparative study of texture measures for terrain classification, IEEE Trans. Syst. Man. Cybern. 4 (1976) 269–285.
G.D. Tourassi, Journey toward computer-aided diagnosis: role of image texture analysis, Radiology 213 (1999) 317–320.
N.R. Mudigonda, R.M. Rangayyan, J.L. Desautels, Gradient and texture analysis for the classification of mammographic masses, IEEE Trans. Med. Imaging 19 (2000) 1032–1043.
N.R. Mudigonda, R.M. Rangayyan, J.L. Desautels, Detection of breast masses in mammograms by density slicing and texture flow-field analysis, IEEE Trans. Med. Imaging 20 (2001) 1215–1227.
A. Kadir, L.E. Nugroho, A. Susanto, P.I. Santosa, Performance improvement of leaf identification system using principal component analysis, Int. J. Adv. Sci Technol. 44 (2012) 113–124.
J. Virmani, V. Kumar, N. Kalra, N. Khandelwal, Neural network ensemble based CAD system for focal liver lesions from B-mode ultrasound, J. Digit. Imaging 27 (2014) 520–537.
Kriti, J. Virmani, R. Agarwal, Evaluating the efficacy of Gabor features in the discrimination of breast density patterns using various classifiers, in: N. Dey et al., (Ed.), Classification in BioApps, vol. 26, Springer, 2018, pp. 105–131.
Kriti, J. Virmani, Breast density classification using Laws' mask texture features, Int. J. Biomed. Eng. Technol. 19 (3) (2015) 279–302.
J. Virmani, V. Kumar, N. Kalra, N. Khandelwal, A comparative study of compute raided classification systems for focal hepatic lesions from B-mode ultrasound, J. Med. Eng. Technol. 37 (44) (2013) 292–306.
Kriti, J. Virmani, S. Thakur, Application of statistical texture features for breast tissue density classification, in: A.I. Awad, M. Hassaballah (Eds.), Image Feature Detectors and Descriptors, vol. 630 Springer, 2016, pp. 411–435.
J. Sachdeva, V. Kumar, I. Gupta, N. Khandelwal, C.K. Ahuja, A dual neural network ensemble approach for multi-class brain tumor classification, Int. J. Numer. Method Biomed. Eng. 28 (2012) 1107–1120.
W.L. Lee, K.S. Hsieh, Y.C. Chen, A study of ultrasonic liver images classification with artificial neural networks based on fractal geometry and multiresolution analysis, Biomed. Eng. Appl. Basis Commun. 16 (2004) 59–67.

T.C. Andre, R.M. Rangayyan, Classification of breast masses in mammograms using neural networks with shape, edge sharpness, and texture features, J. Electron Imaging 15 (2006) 013019–013029.
Y. Wu, M.L. Giger, K. Doi, C.J. Vyborny, R.A. Schmidt, C.E. Metz, Artificial neural networks in mammography: application to decision making in the diagnosis of breast cancer, Radiology 187 (1993) 81–87.
H. Sujana, S. Swarnamani, S. Suresh, Application of artificial neural networks for the classification of liver lesions by image texture parameters, Ultrasound Med. Biol. 22 (1996) 1177–1181.
J. Virmani, V. Kumar, N. Kalra, N. Khandelwal, Prediction of cirrhosis based on singular value decomposition of gray level co-occurrence matrix and an neural network classifier, in: Proceedings of the IEEE International Conference on Developments in E-Systems Engineering, Dubai (DeSe), 2011, pp. 146–151.
A.J. Viera, J.M. Garrett, Understanding interobserver agreement: the kappa statistic, Fam. Med. 37 (2005) 360–363.